Langmuir

Article

pubs.acs.org/Langmuir

Anomalous Silica Colloid Stability and Gel Layer Mediated Interactions

Julie L. Bitter,[†] Gregg A. Duncan,[‡] Daniel J. Beltran-Villegas,[‡] D. Howard Fairbrother,[†] and Michael A. Bevan*[,‡]

[†]Department of Chemistry and [‡]Department of Chemical & Biomolecular Engineering, Johns Hopkins University, Baltimore, Maryland 21218, United States

Supporting Information

ABSTRACT: Total internal reflection microscopy (TIRM) is used to measure SiO_2 colloid ensembles over a glass microscope slide to simultaneously obtain interactions and stability as a function of pH (4−10) and NaCl concentration (0.1−100 mM). Analysis of SiO_2 colloid Brownian height excursions yields kT-scale potential energy vs separation profiles, $U(h)$, and diffusivity vs separation profiles, $D(h)$, and determines whether particles are levitated or irreversibly deposited (i.e., stable). By including an impermeable SiO_2 "gel layer" when fitting van der Waals, electrostatic, and steric potentials to measured net potentials, gel layers are estimated to be ∼10 nm thick and display an ionic strength collapse. The $D(h)$ results indicate consistent surface separation scales for potential energy profiles and hydrodynamic interactions. Our measurements and model indicate how SiO_2 gel layers influence van der Waals (e.g., dielectric properties), electrostatics (e.g., shear plane), and steric (e.g., layer thickness) potentials to understand the anomalous high ionic strength and high pH stability of SiO_2 colloids.

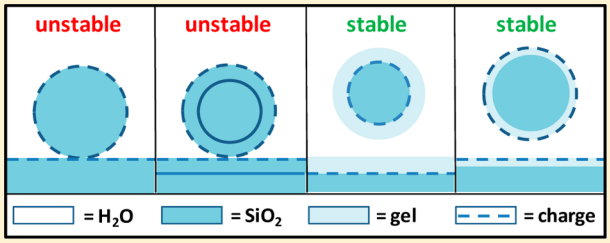

INTRODUCTION

Silica is ubiquitous. It makes up 60% of the earth's crust, and silicates make up 90% of all minerals. It is present in amorphous and crystalline forms important for everyday use, optics, and microelectronics. It is present in food, pharmaceuticals, and organisms. As such, understanding the chemical and physical properties of bulk silica, silica surfaces, and colloidal silica is crucial to numerous applications. A great deal of silica chemistry is well understood and catalogued in the comprehensive book by Iler.[1] However, the stability of colloidal silica against aggregation at high ionic strengths and high pHs is often referred to as "anomalous"[2] because it is not well described by the Derjaguin−Landau−Verwey−Overbeck (DLVO) theory.[3,4]

Historical reviews of possible stabilizing mechanisms that might account for anomalous silica colloid stability are contained within representative papers on the topic.[2,5−8] Direct measurements of force vs distance curves with the surface forces apparatus and the atomic force microscope indicate a short-range repulsion.[5−8] While this measured repulsion appears sufficient to account for anomalous colloidal stability, its physical origin remains an open question. Two mechanisms suggested in the literature include structural forces due to interfacial water[9] or steric interactions between silica gel layers.[10] The water structuring mechanism does not appear to be unique to silica. The presence of silica gel layers is supported by measurements of adhesion, friction, contact angle,[5] and surface density profiles via scattering/spectroscopic methods.[11−13] Despite some evidence in favor of silica gel layers, direct measurements[5−8] do not conclusively support either mechanism or a quantitative potential model. It is also not clear that the role of silica gel layers has been treated self-consistently in terms of their effects on all interactions including van der Waals, electrostatic, and steric interactions.

In this work, we simultaneously measure the interactions and stability of silica colloids over a glass microscope slide as a function of pH (4−10) and ionic strength (0.1−100 mM NaCl). TIRM is used to nonintrusively measure weak kT-scale interactions between a glass microscope slide and an ensemble of silica colloids[14] by analyzing their Brownian height excursions, which also reveals whether they are irreversibly deposited or levitated (i.e., stable). This has the advantage that separation-dependent interactions are obtained simultaneously with measurements of stability, so the two can be unambiguously linked in the same material system. We also simultaneously obtain potential energy vs separation, $U(h)$, and diffusivity vs separation, $D(h)$, profiles by fitting the Smoluchowski equation coefficients to the measured particle dynamic trajectories. The $D(h)$ trajectories yield additional information about particle−wall separation and fluid mechanics important to interpretation of electrostatic and steric interactions. As such, the present study provides new measurements and models of silica gel-layer-mediated interactions that lead to anomalous silica colloid stability.

Received: April 29, 2013
Revised: June 17, 2013
Published: June 18, 2013

THEORY

Potential Energy Profiles. By measuring a statistically significant number of height excursions, h, of a spherical particle above a planar wall surface, a normalized equilibrium height histogram, $p(h)$, can be related to net separation-dependent interaction potential, $U(h)$, via Boltzmann's equation as

$$p(h) = \exp[-U(h)/kT] \tag{1}$$

where k is Boltzmann's constant and T is absolute temperature. Equation 1 can be inverted to obtain a measurement of $U(h)$ from measured $p(h)$ data as

$$U(h) = -kT \ln[p(h)] \tag{2}$$

Theoretical models of $U(h)$ can be computed from superposition of contributing potentials as

$$U(h) = U_G(h) + U_E(h) + U_V(h) + U_S(h) \tag{3}$$

where the subscripts refer to the gravitational (G), electrostatic (E), van der Waals (V), and steric (S) interactions. The gravitational potential is associated with a body force, whereas the other potentials are associated with surface forces. Electrostatic and van der Waals potentials were considered in the original DLVO theory.[3,4]

The gravitational potential energy of each particle depends on its height, h, of the particle above the wall, multiplied by its buoyant weight, G, as given by

$$U_G(h) = Gh = mgh = (4/3)\pi a^3(\rho_p - \rho_f)gh \tag{4}$$

where m is buoyant mass, g is acceleration due to gravity, and ρ_p and ρ_f are particle and fluid densities.

The interaction between electrostatic double layers on two plates (from superposition, nonlinear Poisson–Boltzmann equation, 1:1 monovalent electrolyte)[15] can be used in conjunction with the Derjaguin approximation to give the particle–wall potential as[16]

$$U_E(h) = B \exp[-\kappa h] \tag{5}$$

$$B = 64\pi\varepsilon a\left(\frac{kT}{e}\right)^2 \tanh\left(\frac{e\psi_1}{4kT}\right)\tanh\left(\frac{e\psi_2}{4kT}\right) \tag{6}$$

$$\kappa = \left[\frac{e^2 N_A}{\varepsilon kT}\sum_i (z_i)^2 C_i\right]^{1/2} \tag{7}$$

where κ is the inverse Debye length, ε is the solvent dielectric constant, e is the elemental charge, ψ_1 and ψ_2 are surface potentials, N_A is Avogadro's number, C_i is electrolyte molarity, and z_i is ion valence.

van der Waals attraction between two plates as predicted from the Lifshitz theory[17] (which includes retardation and screening effects) can be used in conjunction with the Derjaguin approximation to give the particle–wall potential as[18]

$$U_V(h) = (a/6)\int_h^\infty -A(l)/l^2 \mathrm{d}l \tag{8}$$

where $A(l)$ is the Hamaker function given by[19,20]

$$A(l) = -\frac{3}{2}kT\sum_{n=0}^{\infty}{}' \int_{r_n}^{\infty} x\{[1 - \Delta_{13}\Delta_{23}e^{-x}] + \ln[1 - \bar{\Delta}_{13}\bar{\Delta}_{23}e^{-x}]\}\mathrm{d}x \tag{9}$$

where the Δ terms include the frequency-dependent dielectric properties of the particle (1), wall (2), and medium (3) and the remainder of the terms are defined in previous papers.[18,19] The prime (′) next to the summation indicates that the first term ($n = 0$) is multiplied by $1/2(1 + 2\kappa l)\exp(-2\kappa l)$ to account for screening of the zero-frequency contribution.

The interaction between surfaces coated with macromolecular layers depends on the free energy change of layers under compression.[21−23] For a layer with a brush architecture on a planar surface with an uncompressed thickness, δ_0, and free energy per area, f_0, the compressed free energy per area, $f(\delta)$, for $1/2 < \delta/\delta_0 < 1$ can be captured accurately by[24]

$$f(\delta)/f_0 = 1 + \Gamma_B \exp[-\gamma_B(\delta/\delta_0)] \tag{10}$$

where Γ_B and γ_B are dimensionless constants specific to the brush architecture.[24] Using this expression in the Derjaguin approximation, the potential between two symmetric macromolecular brush layers as can be obtained as[24]

$$U_{S,B}(h) = 16\pi a f_0 \delta_0(\Gamma_B/\gamma)\exp[-(h\gamma_B/2\delta_0)] \tag{11}$$

For different interfacial macromolecular architectures with different decaying density profiles at their periphery, different values of Γ and γ can be used in eq 10. Because eq 11 can be used to accurately model adsorbed macromolecular layer repulsion for a broad range of δ_0, f_0, Γ, and γ, a general repulsive steric potential of the form

$$U_S(h) = \Gamma \exp(-\gamma h) \tag{12}$$

is broadly applicable (by lumping unknown constants together), particularly when the uncompressed layer properties and architecture are not well characterized (which has also been shown for asymmetric interactions between layers of different properties[24]).

Diffusivity Profiles. In contrast to measuring the equilibrium probability $p(h)$ to obtain $U(h)$ via eq 2, measurements of the time-dependent probability, $p(h,t)$, can be used to obtain both $U(h)$ and the separation-dependent diffusivity, $D(h)$, as described by the Smoluchowski equation[25]

$$\frac{\partial p(h,t)}{\partial t} = \frac{\partial}{\partial h}D(h)\left[\frac{\partial p(h,t)}{\partial h} + \frac{p(h,t)}{kT}\frac{dU(h)}{dh}\right] \tag{13}$$

which reduces to Boltzmann's equation in the long-time limit as equilibrium is approached. In previous work, we reported nonequilibrium analysis of colloidal trajectories to obtain $U(h)$ and $D(h)$. Measured $D(h)$ are modeled using

$$D(h) = D_0 f(h) \tag{14}$$

where D_0 is the Stokes–Einstein coefficient of an unbounded spherical particle given by

$$D_0 = \frac{kT}{6\pi\eta a} \tag{15}$$

where η is the fluid medium viscosity and $f(h)$ accounts for particle–wall hydrodynamic interactions from Brenner,[26] which is accurately captured by the simple expression[27]

$$f(h) = \frac{6h^2 + 2ah}{6h^2 + 9ah + 2a^2} \tag{16}$$

dx.doi.org/10.1021/la401607z | Langmuir 2013, 29, 8835−8844

MATERIALS AND METHODS

Colloids and Surfaces. Hydrochloric acid, potassium hydroxide, sodium chloride (all from Fisher Scientific), and colloidal SiO_2 (nominal diameter of 2.34 μm, Bangs Laboratories) were used as purchased and without further purification. Nonporous amorphous SiO_2 colloids were synthesized by a precipitation method using pure reagents with minimal trace elements. Glass microscope slides (Fisherbrand Plain Microscope Slides) had a manufacturer reported density of 2.48 g/cm^3 and a soda lime composition (approximately 72% silicon dioxide, 14% sodium oxide, 6% calcium oxide, 4% magnesium oxide, 1% aluminum oxide, 1% potassium oxide, <1% other trace elements). Microscope slides were sonicated for 30 min in acetone, 30 min in isopropanol, soaked in Nochromix overnight, and soaked in 0.1 M KOH for 30 min prior to use. Slides were again rinsed with deionized water and dried with nitrogen before use. Colloidal SiO_2 dispersions were prepared by diluting 0.7 μL of the manufacturer stock dispersion into 1 mL of the desired pH and ionic strength solution, which was sonicated for 15 min before diluting 100× before introduction into the measurement cell.

Ensemble Total Internal Reflection Microscopy. All experiments were performed in cells consisting of a 5 mm i.d. Viton O-ring (McMaster Carr) sealed with vacuum grease (Corning) to cleaned microscope slides. A 100 μL of the SiO_2 dispersion was added to the O-ring and covered with a coverslip. Experiments were performed using a Zeiss Axioplan 2 optical microscope with a 40× objective. Particle scattering was recorded with a 12-bit CCD camera (Hamamatsu ORCA-ER) operated in 4-binning mode at ~27.6 fps for 30 000 frames. The evanescent wave was generated by a 15 mW 632.8 nm HeNe laser (Melles Griot) focused onto a dovetail prism (Red Optronics) at an incident angle of 68° to create a decay length of 113.7 nm. Image analysis algorithms[28] coded in FORTRAN were used to track the lateral trajectories and scattering intensity of each particle.

Diffusivity Landscape Analysis. Fitting measured particle dynamics with the Smoluchowski equation (eq 13) to obtain the coefficients (i.e., $U(h)$, $D(h)$) is described in previous[29] and recent[30] papers from our group. Our previous analysis of local dynamics at each elevation provides a more intuitive explanation of how $D(h)$ can be extracted simultaneously with $U(h)$.[29,31] In this work, we employ a less obvious but numerically more robust scheme based on a global analysis of excursions between all elevations to find an optimal fit to the Smoluchowski equation. Development of the global analysis algorithm is described elsewhere,[32] and specific details relevant to colloidal interactions are provided in our recent paper.[30] In brief, a FORTRAN program was used to construct a matrix enumerating the number of times all particles jumped from each initial height to all other heights on a given time scale. Using a Monte Carlo sampling scheme, values of $U(h)$ and $D(h)$ are optimized to fit the measured data. Convergence is determined when $U(h)$ and $D(h)$ fluctuate about a solution that shows a minimum difference with the measured dynamics. The magnitude of the fluctuations about the solution provides an estimate of error bars on the solution.

RESULTS AND DISCUSSION

Example Deviation from DLVO Theory. DLVO theory is used to understand the stability of charged colloids in aqueous media in terms of pair potentials that are the superposition of electrostatic repulsion and van der Waals attraction. However, to demonstrate how DLVO theory can be an oversimplification, even in apparently model systems, Figure 1 shows a measured potential for ~2.1 μm SiO_2 colloids interacting with a glass microscope slide in 20 mM NaCl at pH = 10. As noted in more detail in the Materials and Methods section, the colloids are nonporous, amorphous, pure SiO_2 and the microscope slide has a soda lime glass composition. We chose this system to be representative of typical commercially available silica materials with compositions that might also be encountered in environmental applications. The theoretical prediction using

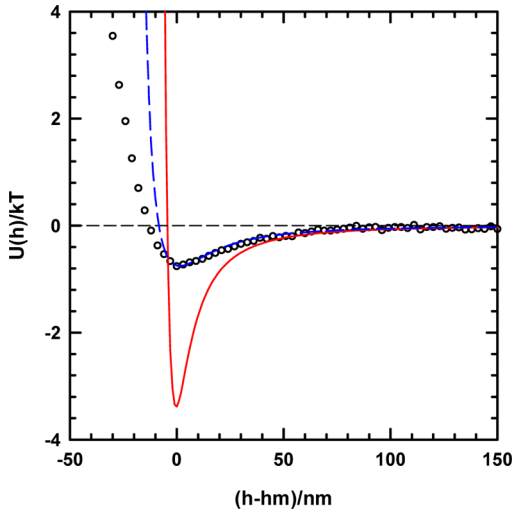

Figure 1. Example of disagreement between ensemble TIRM measured particle−wall potential energy profile (points) and DLVO theory (red solid line) for 2.1 μm SiO_2 in [NaCl] = 20 mM at pH = 10. Addition of a steric potential to the DLVO potentials produces a net potential prediction (blue dashed line) in better agreement with the depth of the minimum.

only electrostatic and van der Waals potentials (eqs 5 and 8) with independently measured parameters displays a deeper secondary minimum than the experimental data and does not match the potential shape. The predicted potential also indicates a lower energy barrier and particle stability against deposition on the wall. This finding is consistent with anomalous SiO_2 colloid stability reported in the past.[2−8]

By simply adding an additional repulsive potential, it is possible to more accurately capture the attractive well depth, shape, and range. As already reviewed in the Introduction, a solvated gel layer, which is also possibly a polyelectrolyte, is thought to provide a stabilization mechanism through a repulsive steric interaction. However, simply introducing a short-range repulsion cannot provide stability in the presence of a long-range van der Waals attraction; the mechanism must be more complex than this simple picture, and it must be physically realistic. In the following, we provide more measurements and potential fits like the one illustrated in Figure 1 to understand the mechanism of silica colloid stability beyond the standard DLVO theory.

Interaction Potentials vs Ionic Strength (at fixed pH = 10). Figure 2A shows potential energy profiles between 2.1 μm SiO_2 colloids interacting with a glass microscope slide at pH = 10 for [NaCl] = 0.1−85 mM. The gravitational potential energy, which corresponds to a body force, has been subtracted from the measured potential energy profiles to leave only the contributions due to colloidal/surface forces. The remaining net potentials display the correct qualitative trend based on expectations that the range of electrostatic repulsion decreases with increasing ionic strength to reveal a shorter range attractive interaction. However, quantitative curve fits to the net interaction potentials, which are discussed in detail in the following sections, are not accurately captured for all conditions by DLVO potentials alone.

To analyze the measured interactions reported in Figure 2A, the net potentials were fit with either DLVO potentials only (eq 3 with $U_E + U_V$) shown by solid lines or DLVO plus a steric contribution (eq 3 with $U_E + U_V + U_S$) shown by dashed lines.

dx.doi.org/10.1021/la401607z | Langmuir 2013, 29, 8835−8844

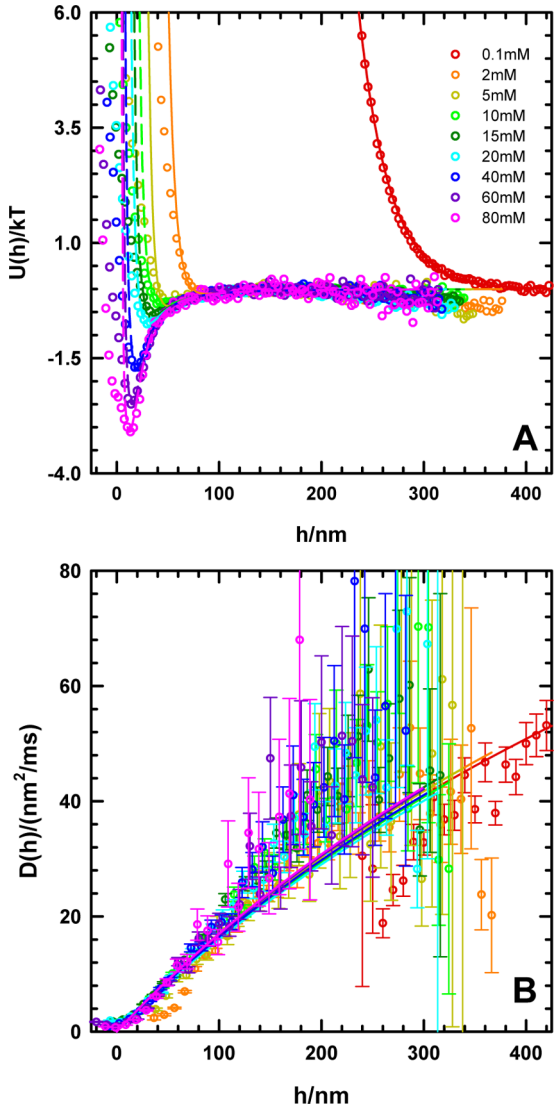

Figure 2. Ensemble TIRM measurements of (A) potential energy profiles, $U(h)$, and (B) diffusivity profiles, $D(h)$, for 2.1 μm SiO_2 at pH = 10 with [NaCl] = 0.1−100 mM. Color scheme for lines and points indicates [NaCl] given in the legend in A. In A, the points are measured data from an equilibrium analysis of particle trajectories using eq 1, solid lines indicate DLVO potentials only (eq 3 with $U_E + U_V$), and dashed lines indicate DLVO plus a short-range steric contribution (eq 3 with $U_E + U_V + U_S$). In B, the points are measured data from a nonequilibrium analysis of particle trajectories using eq 13, solid lines are fits to theoretical predictions from eq 14, and error bars are explained in the Materials and Methods section.

DLVO potentials were fit to the measured profiles for [NaCl] = 0.1−5 mM, and DLVO plus a steric potential was fit to measured profiles for [NaCl] = 10−85 mM. Solid lines representing purely DLVO interactions were obtained without any adjustable parameters using independent measurements of the solution conductivity and pH to predict κ from eq 7 and ψ using a literature model summarized in the Supporting Information.[33,34] Although the SiO_2 ψ values in our experiments could differ from this literature model based on different compositions or cleaning procedures, we proceed with this model to minimize adjustable parameters and ultimately show it captures our measured DLVO potentials without modification. The van der Waals attraction was modeled using literature dielectric properties for water and SiO_2 described in our previous work.[18,35] The agreement of the measured potentials at low ionic strengths with DLVO theory is consistent with previous TIRM measurements of interactions between different colloidal materials including SiO_2 colloids and glass surfaces.[14,36] We return to a discussion of the non-DLVO potential fits after first presenting measurements of separation-dependent diffusivity profiles, $D(h)$, to provide additional information on the SiO_2 particle−wall interaction.

Hydrodynamic Interactions vs Ionic Strength (at fixed pH = 10). As part of verifying both the DLVO and the non-DLVO potential fits in Figure 2A, it is useful to have an independent measurement of absolute separation between the particle and the wall. In Figure 2B, we report measurements of particle diffusivity profiles, $D(h)$, obtained from a dynamic analysis based on eq 13 (see Materials and Methods). This analysis also yields potential energy profiles, $U(h)$, essentially identical to those obtained with the standard Boltzmann inversion in eq 2. This confirms the dynamic analysis successfully recovers the potential energy due to conservative forces, which provides confidence in the $D(h)$ data obtained simultaneously in this analysis.

Figure 2B shows fit theoretical $D(h)$ curves using the literature value for the viscosity of water and the particle radius obtained from the gravitational potential energy fit (eq 4, subtracted from data in Figure 2A). By fitting the measured $D(h)$ curves to the theoretical prediction in eqs 14−16, we obtain an estimate of the absolute separation scale by setting h = 0 as the location where $D(h)$ = 0. By measuring and fitting the complete functional form of $D(h)$, we obtain a more accurate estimate of separation than previous measurements of spatially averaged diffusivities.[27] The $D(h)$ data become scattered at larger separations due to increasing signal noise and lower statistical sampling (at corresponding higher energies in the $U(h)$ data), but the curve fits display good agreement with the less noisy data at short separations.

For the [NaCl] = 0.1−5 mM data fit with only DLVO potentials ($U_E + U_V$) in Figure 2A, the particle−wall absolute separation scales from the $U(h)$ and $D(h)$ fits are in good agreement with no adjustable parameters (see Table 1 and Figure S1, Supporting Information). Specifically, the location of the most probable separation, h_m, at the potential energy minimum, and where the sum of the forces equal zero, is similar in both the DLVO potential fits to the $U(h)$ data using eq 3 and the hydrodynamic interaction model fits to the $D(h)$ data using eq 14. As already noted, this finding is consistent with numerous previous TIRM studies that report excellent agreement with DLVO theory at low ionic strengths[14,18,27,36,37]

Table 1. Constants Used in Theoretical Fits

variable (units)	value	equation
ρ_p (g/cm^3)	1.96	4
ρ_f (g/cm^3)	1.00	4
ϵ_w	78	7
T (K)	295	7
η (Pa·s)	1.002×10^{-3}	15
A_0 (kT)	1.501	17
a_f (kT)	1.962	18
b_f (kT·nm^{-1})	0.0281	18
c_f (nm^{-1})	0.0593	18
d_f (nm^{-2})	0.0033	18

dx.doi.org/10.1021/la401607z | Langmuir 2013, 29, 8835−8844

as well as measurements that have confirmed the accuracy of the theoretical expression for $D(h)$.[27,38,39] When fitting the DLVO + steric potentials to the data for [NaCl] > 10 mM in Figure 2A, we also use $D(h)$ data to confirm the validity of the separation scale inferred from the conservative forces and confirm some assumptions about the fluid flow in the presence of gel layers. Before discussing the potential fits that include steric contributions in Figure 2A, we first discuss several conceptual issues related to including a gel layer in a manner that consistently treats electrostatic and van der Waals potentials.

Role of "Gel" Layer in van der Waals, Electrostatic, and Steric Potentials. The primary conceptual issue to address for computing net potentials in the presence of silica gel layers is the reference separation for each potential. Four illustrative cases are depicted in Figure 3 showing (1) no gel layer with U_E and U_V on a scale, h, between the H_2O/SiO_2 interfaces, (2) a gel layer composed of nearly pure SiO_2 with U_E and U_V on the h scale and a steric interaction, U_S, on a separation scale, L, between the SiO_2 gel/bulk interfaces, (3) a gel layer with mostly water properties that is permeable to fluid flow and has charge on the SiO_2 gel/bulk interfaces (this suggests U_E, U_V, and U_S should all be on the L scale), and (4) a gel layer with mostly water properties that is impermeable to fluid flow and has a no-slip surface/potential originating on the H_2O/SiO_2 gel interfaces (this suggests U_V and U_S should be on the L scale and U_E should be on the h scale). This list is not exhaustive, but these are the four physically meaningful cases that bound other cases including gel layer dielectric properties intermediate to pure H_2O/pure SiO_2 and/or charge distributed (and a shear plane) between the H_2O/SiO_2 and the SiO_2 gel/bulk interfaces.

These cases can be compared and contrasted to decide on an appropriate model for the net potentials in Figure 2A. Case 1 is the standard model for the DLVO theory. Case 2 illustrates a gel layer that has no stabilizing effect. In particular, if the gel layer is composed almost entirely of SiO_2, the van der Waals attraction will still be as strong on the h scale as in case 1.[40−42] However, since steric repulsion between the gel layers is not generated until $h = 0$, the strong van der Waals attraction for $h > 0$ would cause irreversible surface adhesion. In fact, cases 1 and 2 have the same van der Waals and electrostatic interactions, but the repulsion at contact is weaker (soft steric repulsion instead of hard wall repulsion). Clearly a different mechanism is required to produce stabilization by a silica gel layer.

Cases 3 and 4 illustrate gel layers with a predominantly water composition and therefore water dielectric properties. This effectively weakens van der Waals on the h scale by moving U_V to the L scale in the limit of a purely water layer. The difference between cases 3 and 4 is whether the electrostatic potential originates at the SiO_2 gel/bulk interfaces (case 3) or the H_2O/SiO_2 gel interfaces (case 4). These cases are limits of intermediate cases that depend on whether the layer is a polyelectrolyte, how charge is spatially distributed within the layer, and whether ions are mobile within the layer.[10,43] Both of these cases can produce net potentials that correspond to stable particles and can be fit to the data in Figure 2A. In short, case 4 has more electrostatic repulsion and as a result has a smaller steric contribution, whereas case 3 has less electrostatic repulsion and therefore requires a greater steric contribution. The key effect in cases 3 and 4 compared to case 2 is that van der Waals attraction is weaker due to the gel layer.

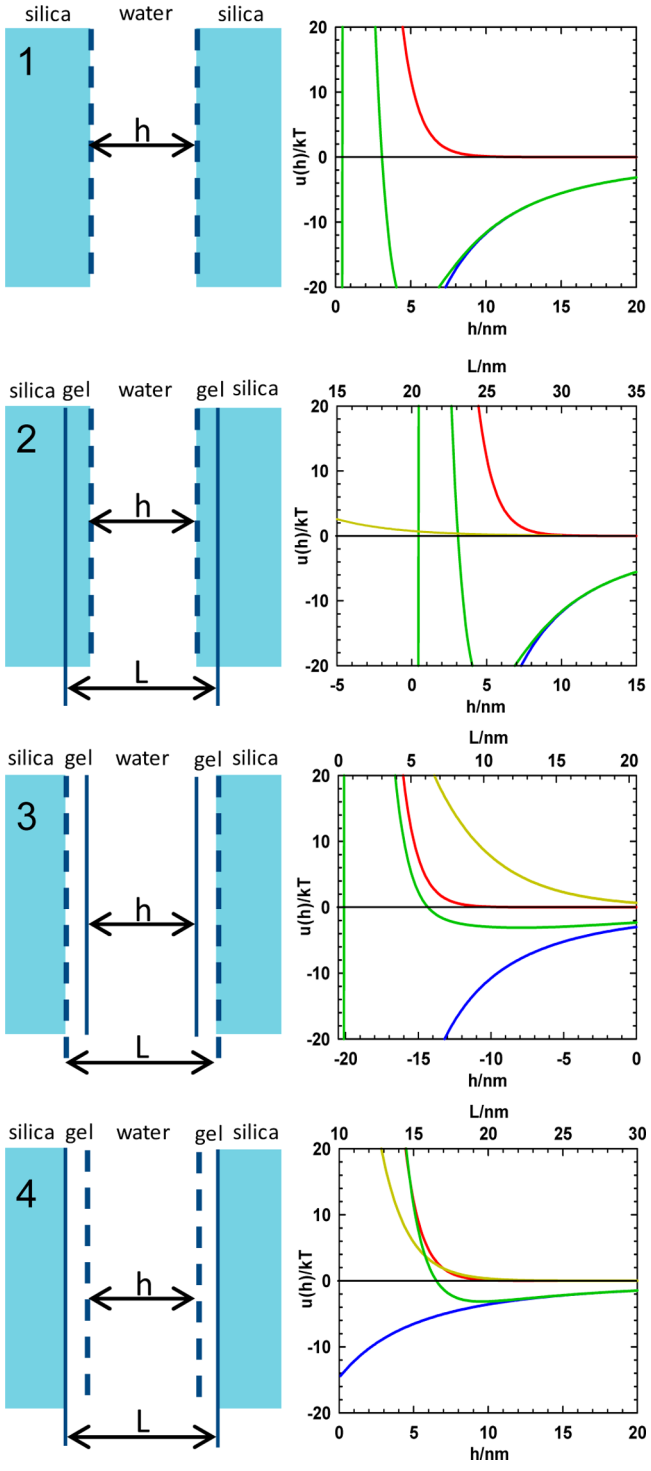

Figure 3. Schematics and predicted potentials (for pH = 10, [NaCl] = 80 mM in Figure 2A) based on various cases for including SiO_2 gel layers. In the schematics and predictions, h is the separation between the outer edges of the SiO_2 gel layers (i.e., the H_2O/SiO_2 gel interfaces) and L is the separation between the inner edges of the SiO_2 gel layers (i.e., the SiO_2 gel/bulk interface). See text for detailed explanation of each case, but in brief (top-to-bottom) (1) the typical configuration with no gel layers considered in the DLVO theory, (2) gel layers of mostly SiO_2 composition, (3) gel layers of mostly H_2O composition that are permeable to fluid flow, (4) gel layers of mostly H_2O composition that are impermeable to fluid flow. Potentials are color coded as electrostatics (red), van der Waals (blue), steric (yellow), and net (green).

dx.doi.org/10.1021/la401607z | Langmuir 2013, 29, 8835−8844

Fitting DLVO and Steric Interactions in the Presence of a "Gel" Layer. Based on the discussion of the different cases in Figure 3, the measured profiles for [NaCl] > 10 mM in Figure 2A are fit using models based on cases 3 and 4. As in the purely DLVO fits for [NaCl] < 5 mM, the same ionic strength and pH-dependent κ from eq 7 and the ψ model in the Supporting Information[27,28] are used in the DLVO potentials for [NaCl] > 10 mM. For the steric potential in eq 12, a prefactor of $\Gamma = 100kT$ is assumed and the steric inverse decay length, γ, becomes the sole adjustable parameter in the net potential. While $\Gamma = 100kT$ is somewhat arbitrary, it is of the correct order of magnitude based on the few cases where the steric prefactor has been estimated[22] and based on what is necessary to generate the observed stability. We decided to fix $\Gamma = 100kT$ for several reasons including (1) a greater sensitivity of the fit to the decay length than the prefactor when both parameters are varied, (2) some uncertainty in the strong, short-range repulsion due to noise, which affects estimates of the intercept, and (3) the prefactor in steric interactions cannot generally be predicted a priori based on independent parameters.[22] On the basis of this prefactor, the gel layer thickness, Δ, can be estimated as $2\Delta = L - h = 5\gamma^{-1}$, which corresponds to a decay from $100kT$ to $\sim 0.5kT$ based on the properties of the exponential function. As a result, the difference between cases 3 and 4 is simply whether all potentials are on the same separation scale (case 3) or whether the electrostatic potential is shifted outward by $5\gamma^{-1}$ (case 4). We return to a discussion of the validity of the assumed prefactor after reporting and discussing the fit steric decay lengths.

Figure 4 reports the inferred decay lengths, γ^{-1}, and gel thicknesses, $\Delta = 0.5(L - h) = 2.5\gamma^{-1}$, as a function of ionic strength from the fits to the pH = 10 profiles in Figure 2. Data corresponding to fits based on case 3 indicate decay lengths of $\gamma^{-1} \approx 4-7$ nm and thicknesses of $\Delta \approx 10-17$ nm, whereas fits based on case 4 give $\gamma^{-1} \approx 2-4$ nm and $\Delta \approx 5-10$ nm. It should be noted that these fit parameters are obtained by generating a repulsion that results in the correct attractive well depth, which then determines the potential energy minimum location at the most probable separation, h_m. This approach is necessary since the actual repulsive decay corresponds to a strong force approaching the noise limit of the TIRM method,[44,45] which limits the accuracy of the measured repulsive decay length. In short, noise softens strong forces (i.e., large energy changes over small distances) at short separations and high ionic strengths, so that matching the potential energy minimum well depth and location is a better measure of the net repulsion than the decay length.

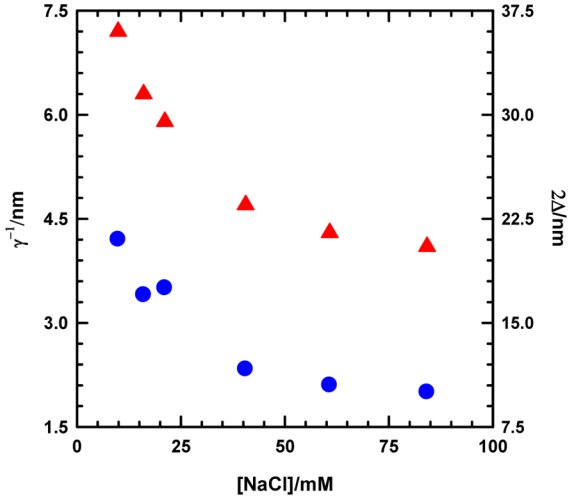

Figure 4. Steric decay length, γ^{-1} (left), and twice the single gel layer thickness, 2Δ (right), vs [NaCl]/mM at pH = 10 from fits in Figure 2A based on models for cases 3 (red triangles) and 4 (blue circles) in Figure 3.

When considering the absolute values of the layer dimensions inferred in Figure 4, it is important to recall that cases 3 and 4 bound some limiting physical models. For example, distributing charge anywhere in between the SiO_2 gel/bulk interfaces (case 3) or the H_2O/SiO_2 gel interfaces (case 4) would produce gel layer estimates in between the two curves shown in Figure 4. If the layers contain a higher concentration of SiO_2 than the nearly pure H_2O layers in cases 3 and 4 then the two cases in Figure 4 represent lower bounds where the layer thickness would diverge to infinity as the layers approach pure SiO_2 (as in case 2 where the gel layer is not capable of generating a stabilizing repulsion beyond the range of van der Waals attraction). One way to overcome this problem is to also include surface roughness in addition to the gel layer, which will weaken van der Waals[18] and still allow gel layers without pure water properties.[46,47]

Do Inferred Gel Layer Properties Make Sense? The inferred gel layers in Figure 4 from the measured potentials in Figure 2 display the expected trend by showing a decreasing thickness vs increasing ionic strength. This behavior is consistent with the gel behaving as a polyelectrolyte where screening of electrostatic repulsion within the layers allows for a dimensional collapse.[48,49] It is also expected that this collapse will not occur until high ionic strengths when the Debye length is on the order of the separation of charges within the gel layer. This dimensional collapse will expel water from the gel layer and enrich it in pure SiO_2 properties, which is reminiscent of solvent-quality-mediated collapse of adsorbed polymer layers.[42,46,50,51] Such a collapse will reduce stability by both decreasing steric repulsion and increasing the van der Waals attraction due to changing layer dielectric properties.[42]

The observed stability behavior also has the character of a solvent quality mediated collapse of a repulsive steric interaction. Specifically, an attractive energy minimum evolves beyond the range of an infinitely repulsive steric barrier, which progressively increases bond lifetimes with an exponential dependence on well depth.[24,43] When the attractive well is deep enough to produce most probable bond lifetimes longer than the observation time, then the particle appears to be irreversibly deposited. This type of destabilization mechanism contrasts the typical mechanism for only DLVO interactions, where the height of an energy barrier determines the probability of forming an irreversible bound state involving strong van der Waals attraction at contact. Our results appear to display stability behavior consistent with a decreasing range of steric repulsion due to collapsing impenetrable gel layers.

The values of the inferred thicknesses are larger than the ~2 nm estimates from mechanical force measurements (e.g., SFA,[5] AFM[6]) but comparable to gel thicknesses obtained from surface spectroscopic/scattering methods (e.g., nuclear resonance profiling,[11] neutron, X-ray reflectivity[12,13]). One way to reconcile the differences between layer thicknesses inferred from SFA and AFM force profiles and the TIRM potential energy profiles in Figure 2A is the much higher sensitivity to

dx.doi.org/10.1021/la401607z | Langmuir 2013, 29, 8835−8844

small energies (and forces) with TIRM.[37] In particular, very weak steric interactions between silica gel layers could go undetected with mechanical methods until they generate ≥10 pN of repulsion. In contrast, TIRM is capable of detecting the very onset of silica gel layer compression on the kT energy scale and fN force scale (e.g., 1 kT/100 nm ≈ 10 fN). This sensitivity can be expected to produce thicker layer estimates, and because TIRM is not mechanically limited, it might produce estimates closer to nonintrusive spectroscopic/scattering methods. In short, the 5−17 nm SiO_2 gel layers are reasonable based on literature neutron and X-ray measurements.[12,13]

It is also useful to consider the $D(h)$ data and fits in Figure 2B. The $D(h)$ fits serve the purpose of confirming that steric potentials occur on separation scales consistent with hydrodynamically measured surface separation. In particular, estimates of h_m from non-DLVO fits to $U(h)$ data in Figure 2A for both cases 3 and 4 agree with h_m estimates from the $D(h)$ fits in Figure 2B within the uncertainty of the measurements (see Figure S1, Supporting Information). The pH = 10, [NaCl] = 80 mM potentials in Figure 3 can be used to illustrate this point; the net potential in Figure 3C for case 3 has L_m = 13 nm, whereas the net potential in Figure 3D for case 4 has h_m = 8 nm, which are both within the uncertainty of h_m = 7 nm from the $D(h)$ fit in Figure 2B (it should be noted that L_m and h_m are used in this example since L is the hydrodynamic separation scale in case 3 and h is the hydrodynamic separation scale in case 4). As a result, steric potentials with Γ = 100 kT and layer thicknesses of $\Delta = 2.5\gamma^{-1}$ produce net $U(h)$ profiles on the same separation scale as the $D(h)$ data and fits. However, the $D(h)$ fits do not resolve difference between cases 3 and 4.

Of cases 3 and 4 presented in Figure 3, case 4 is more likely for several reasons. Because the electrostatic repulsion is longer range in case 4, the silica gel layer thicknesses in case 4 are thinner and closer to the estimates from spectroscopic/scattering methods. On the basis of previous measurements of adsorbed polymers,[46] it is more likely the gel layers are impermeable to flow (case 4). The electrostatic potential appears more likely to originate from a surface potential at the outer edge of the silica gel layer (case 4).

Potentials and Stability vs Ionic Strength and pH. To understand how the silica gel layer influences stability as a function of both pH and ionic strength, Figure 5 reports results that summarize both stability and potential energy profile measurements. In addition to the pH = 10 results already discussed in Figures 2−4, ionic-strength-dependent results are shown for pHs of 7, 5.5, and 4. The points show several states indicating whether (1) all particles were robustly levitated throughout the entire observation time and had potentials captured by DLVO theory (green circles), (2) all particles were robustly levitated and had potentials that required DVLO theory + a steric repulsion (green triangles), (3) some particles became irreversibly deposited during the observation time and the particles that remained levitated had potentials that required DVLO theory + a steric repulsion (yellow inverted triangles), or (4) all particles were irreversibly deposited during the observation time (red squares). The measured ionic-strength-dependent potentials for each pH are included in Figures S4−S6, Supporting Information, with fit parameters reported in Table 2. The agreement between measured potentials and theoretical fits for other pHs in Figures S4−S6, Supporting Information, is similar to the agreement observed for the pH = 10 data in Figure 2A.

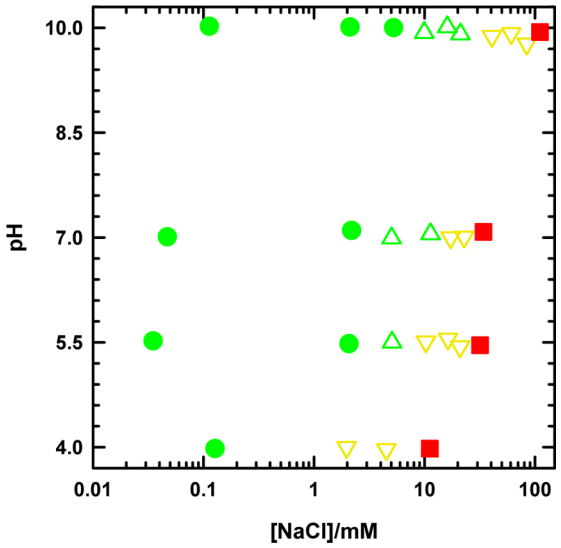

Figure 5. Summary of whether DLVO theory fit measured potentials and the degree of particle stability vs solution pH and [NaCl]. Points indicate (1) robust levitation, accurately modeled by DLVO theory (green circles), (2) robust levitation, modeled by DLVO + steric repulsion (green triangles), (3) slow deposition of particles, levitated particles are modeled by DLVO + steric repulsion (yellow inverted triangles), and (4) irreversible deposition (red squares).

At each pH, there is a clear progression with increasing ionic strength through states 1−4 described in the previous paragraph. The ionic strength dependence is different at each pH showing a more compressed transition through states 1−4 at lower pHs. For example, at pH = 10 the transition from stable particles described by DLVO theory to irreversibly deposited particles occurs between [NaCl] = 5 and 100 mM, whereas the same transition occurs at pH = 4 between [NaCl] = 0.1 and 10 mM. At each pH, the potentials and stability are well described by DLVO theory at low ionic strengths, but an additional repulsion, presumably due to steric gel layer interactions, is required to fit the measured potentials and capture the stability at high ionic strengths.

The agreement between measured low ionic strength potentials with DLVO theory is easy to understand at all pHs; the long-range electrostatic repulsion does not allow particle−wall separations to become small enough to observe a steric repulsion between silica gel layers in contact. However, as the ionic strength is increased at each pH, steric repulsion is required to capture the observed repulsion, lack of attraction, and stability at higher ionic strengths. The fits to measured potentials at all pHs and ionic strengths (Figure 2A, Figures S4−S6, Supporting Information) have no adjustable parameters in the electrostatic and van der Waals contributions using κ from eq 7 and the ψ model in the Supporting Information.[27,28]

The different trends at each pH in Figure 5 are accounted for by the ionic strength and pH dependence of the van der Waals and electrostatic potentials, which suggests the silica gel layer repulsion that is relatively insensitive to pH. This is perhaps most readily illustrated by noting the steric decay length vs solution ionic strength is essentially the same for each pH within the limits of uncertainty of the fit points (see γ^{-1} data in Table 2). Because intramolecular electrostatic repulsion within a polyelectrolyte brush determines its degree of swelling,[48] decreasing such interactions either by screening at elevated ionic strengths or by reducing the total charge via pH-

dx.doi.org/10.1021/la401607z | Langmuir 2013, 29, 8835−8844

Table 2. Experimental Parameters for Each pH and Ionic Strength Condition Examined[a]

pH	2a (μm)	NaCl (mM)	κ^{-1} (nm)	pH	$-\Psi$(mV)	γ^{-1}(#3) (nm)	h_m-U (nm)	γ^{-1} (#4) (nm)	h_m-U (nm)	h_m-D (nm)
10	2.17	0.11	30.0	10.02	120	-	320.5	-	320.5	300
	2.15	2.1	6.6	10.01	100	-	76.4	-	76.4	80
	2.15	5.2	4.2	10.00	83	-	48.1	-	48.1	50
	2.16	9.9	3.0	9.93	61	7.2	39.2	4.2	33.4	45
	2.13	16.1	2.5	10.01	44	6.3	35.1	3.4	25.9	30
	2.17	21.1	2.1	9.91	36	5.9	29.7	3.5	21.5	25
	2.13	40.6	1.5	9.88	26	4.7	17.6	2.33	11.6	15
	2.15	60.8	1.2	9.92	25	4.3	14.1	2.1	9.1	7
	2.15	84.2	1.1	9.77	24	4.1	13.4	2.0	7.5	7
	×	111	0.96	9.94	24	×	×	×	×	×
7	2.13	0.05	44.2	7.01	94	-	443.6	-	443.6	
	2.22	2.2	6.8	7.10	85	-	76.7	-	76.7	
	2.20	5.0	4.3	6.99	70	7.0	47.6	3.1	47.8	
	2.15	11.3	3.0	7.05	49	6.7	37.7	2.6	30.6	
	2.13	17.2	2.5	7.00	36	6.4	35.4	3.4	23.8	
	2.08	22.8	2.1	7.01	30	5.5	25.1	2.7	18.4	
	×	34.1	1.8	7.08	25	×	×	×	×	
5.5	2.22	0.04	51.2	5.52	70	-	480.0	-	480.0	
	2.10	2.1	6.8	5.48	64	-	73.6	-	73.6	
	2.08	5.1	4.3	5.50	54	8.2	53.0	2.7	47	
	2.07	10.3	3.0	5.51	40	8.5	47.8	7.0	30.3	
	2.02	16.3	2.5	5.55	30	6.8	34.8	4.8	21.6	
	2.08	20.9	2.1	5.44	24	7.6	43.3	6.0	20.3	
	×	31.8	1.8	5.46	19	×	×	×	×	
4	2.18	0.13	29.9	3.98	30	-	245.7	-	245.7	
	2.13	2.0	6.6	4.00	29	10.0	67.7	3.0	62.6	
	2.03	4.5	4.2	3.97	25	9.3	57.6	4.0	39.7	
	×	11.1	3.0	3.98	15	×	×	×	×	

[a]The column labeled "γ^{-1} (#3)" is the steric decay length from a net potential fit based on case 3 in Figure 3 and "γ^{-1} (#4)" is the steric decay length from a net potential fit based on case 4. Column labeled as h_m-U is the most probable particle−wall separations obtained from potential energy profile fits, and h_m-D is the most probable height from diffusivity profile fits. Dashes indicate cases without a steric contribution, and "×"s indicate irreversibly deposited particles where potential energy and diffusivity profiles could not be measured.

dependent weak acid groups could produce a dimensional collapse of the layers and an associated decreasing steric repulsion. The steric interaction indeed appears to weaken as the Debye length changes from ∼5 to <1 nm, which is consistent with the screening length becoming comparable to spatial dimensions of intramolecular charge separation within the gel layer to cause its dimensional collapse.[48] By analogy, it might be expected that decreasing charge density with decreasing pH might also influence the average charge separation and intramolecular electrostatic repulsion within the gel layers to also cause a dimensional collapse. Although it is nontrivial to demonstrate quantitatively, we speculate that the average charge separation (i.e., inverse of charge density) is smaller than the characteristic range of intramolecular electrostatic repulsion for pH > 4 so that γ^{-1} does not change in this pH range (but might be expected to decrease as pH is lowered further). Ultimately, the results in Figure 5 in addition to the results in Figures 2−4 show potentials and stability that are well described by a silica gel layer that reduces van der Waals attraction, preserves electrostatic repulsion, and contributes an additional steric repulsion.

CONCLUSIONS

TIRM was used to measure SiO_2 colloid ensembles on a glass microscope slide to simultaneously obtain particle−wall potential energy profiles, diffusivity profiles, and stability as a function of ionic strength and pH. To interpret the measured potentials and explain anomalous high ionic strength stability, a model was developed based on electrostatic and van der Waals potentials from the DLVO theory plus a steric repulsion attributed to silica gel layers on the particle and wall. For such a model to successfully quantify the measured potentials, the van der Waals attraction must be weakened by a layer that has some solvent composition rather than pure silica properties, although surface roughness could account for some weakening. By including an impermeable gel layer when fitting van der Waals, electrostatic, and steric potentials to measured net potentials, gel layer thicknesses of 5−10 nm were obtained from the model, consistent with literature scattering measurements. Such gel layers also indicate consistent surface separation scales for both potential energy profiles and diffusivity profiles based on theoretical models. The net potential model reported here accurately captures measured potentials and stability for [NaCl] = 0−100 mM and pH = 4−10 by including a gel layer that collapses at high ionic strengths but is relatively insensitive to pH. Our findings indicate a model of silica gel layers that captures measured van der Waals, electrostatic, steric, and hydrodynamic interactions and their role in the anomalous high ionic strength stability of silica colloids.

APPENDIX

Here we describe a curve fit to $A(l)$ computed by the Lifshitz theory (eq 9). The form of the expression provides an accurate representation of both retardation and screening effects

dx.doi.org/10.1021/la401607z | Langmuir 2013, 29, 8835−8844

captured by the Lifshitz theory. This expression is convenient for computing the van der Waals potential via the Derjaguin approximation (eq 8) while avoiding the complexity and computational expense of recomputing $A(l)$ from eq 9 each time. The form we choose is

$$A(l) = (1/2)[1 + 2\kappa l]\exp[-2\kappa l]A_0 + A_{1\infty}(l) \quad (17)$$

where A_0 is obtained from eq 9 for $n = 0$ (without the prefactor of $1/2(1 + 2\kappa l)\exp(-2\kappa l)$ indicated by the prime symbol) and $A_{1\infty}(l)$ is obtained from eq 9 for $n = 1-\infty$. This form accounts for the fact that the zero frequency term ($n = 0$) is screened but not retarded and all higher frequency terms ($n > 0$) are not screened but are retarded. The function of $A_{1\infty}(l)$ is accurately fit by

$$A_{1\infty}(l) = (a_f + b_f l)/(1 + c_f l + d_f l^2) \quad (18)$$

where the constants A_0, a_f, b_f, c_f, and d_f are reported in Table 1. Figure S2, Supporting Information, shows the expression in eq 17 accurately captures of $A(l)$ curves computed using the Lifshitz theory (eq 9).

■ ASSOCIATED CONTENT

Supporting Information

Modeling of solution pH and ionic strength and surface potentials as well as additional figures described in the text. This material is available free of charge via the Internet at http://pubs.acs.org.

■ AUTHOR INFORMATION

Corresponding Author

*E-mail: mabevan@jhu.edu.

Notes

The authors declare no competing financial interest.

■ ACKNOWLEDGMENTS

We acknowledge financial support by the National Science Foundation (CHE-1112335, CBET-1066254).

■ REFERENCES

(1) Iler, R. K. *The Chemistry of Silica*; Wiley: New York, 1979; p 866.

(2) Healy, T. W. Stability of Aqueous Silica Sols. In *The Colloid Chemistry of Silica*; American Chemical Society: Washington, DC, 1994; Vol. *234*, pp 147−159.

(3) Derjaguin, B. V.; Landau, L. Theory of the stability of strongly charged lyophobic sols and of the adhesion of strongly charged particles in solutions of electrolytes. *Acta Physicochim. URSS* **1941**, *14*, 633−662.

(4) Verwey, E. J. W.; Overbeek, J. T. G. *Theory of the stability of lyophobic colloids*; Elsevier: Amsterdam, 1948.

(5) Vigil, G.; Xu, Z. H.; Steinberg, S.; Israelachvili, J. Interactions of Silica Surfaces. *J. Colloid Interface Sci.* **1994**, *165* (2), 367−385.

(6) Adler, J. J.; Rabinovich, Y. I.; Moudgil, B. M. Origins of the Non-DLVO Force between Glass Surfaces in Aqueous Solution. *J. Colloid Interface Sci.* **2001**, *237* (2), 249−258.

(7) Valle-Delgado, J. J.; Molina-Bolivar, J. A.; Galisteo-Gonzalez, F.; Galvez-Ruiz, M. J.; Feiler, A.; Rutland, M. W. Hydration forces between silica surfaces: Experimental data and predictions from different theories. *J. Chem. Phys.* **2005**, *123* (3), 034708−12.

(8) Grabbe, A.; Horn, R. G. Double-Layer and Hydration Forces Measured between Silica Sheets Subjected to Various Surface Treatments. *J. Colloid Interface Sci.* **1993**, *157* (2), 375−383.

(9) Derjaguin, B. V.; Churaev, N. V. Structural component of disjoining pressure. *J. Colloid Interface Sci.* **1974**, *49* (2), 249−255.

(10) Tadros, T. F.; Lyklema, J. Adsorption of potential-determining ions at the silica-aqueous electrolyte interface and the role of some cations. *J. Electroanal. Chem. Interfacial Electrochem.* **1968**, *17* (3−4), 267−275.

(11) Lanford, W. A.; Davis, K.; Lamarche, P.; Laursen, T.; Groleau, R.; Doremus, R. H. Hydration of soda-lime glass. *J. Non-Cryst. Solids* **1979**, *33* (2), 249−266.

(12) Richardson, R. M.; Dalgliesh, R. M.; Brennan, T.; Lovell, M. R.; Barnes, A. C. A neutron reflection study of the effect of water on the surface of float glass. *J. Non-Cryst. Solids* **2001**, *292* (1−3), 93−107.

(13) Brennan, T.; Dalgliesh, R. M.; Lovell, M. R.; Richardson, R. M.; Barnes, A. C.; Sergeant, S. A. An X-ray and Neutron Reflection Study of Water Penetration into Fluorocarbon Doped Silica Gel Films. *Langmuir* **2003**, *19* (19), 7761−7767.

(14) Wu, H. J.; Bevan, M. A. Direct Measurement of Single and Ensemble Average Particle-Surface Potential Energy Profiles. *Langmuir* **2005**, *21* (4), 1244−1254.

(15) Russel, W. B.; Saville, D. A.; Schowalter, W. R. *Colloidal Dispersions*; Cambridge University Press: New York, 1989.

(16) Bike, S. G.; Prieve, D. C. Measurements of Double-Layer Repulsion for Slightly Overlapping Counterion Clouds. *Int. J. Multiphase Flow* **1990**, *16* (4), 727−740.

(17) Dzyaloshinskii, I. E.; Lifshitz, E. M.; Pitaevskii, L. P. The general theory of van der Waals forces. *Adv. Phys.* **1961**, *10*, 165−209.

(18) Bevan, M. A.; Prieve, D. C. Direct measurement of retarded van der Waals attraction. *Langmuir* **1999**, *15* (23), 7925−7936.

(19) Prieve, D. C.; Russel, W. B. Simplified Predictions of Hamaker Constants from Lifshitz Theory. *J. Colloid Interface Sci.* **1988**, *125*, 1.

(20) Parsegian, V. A. *Van der Waals Forces*; Cambridge University Press: Cambridge, 2005.

(21) Milner, S. T. Compressing Polymer Brushes-a Quantitative Comparison of Theory and Experiment. *Europhys. Lett.* **1988**, *7* (8), 695−699.

(22) Milner, S. T. Polymer Brushes. *Science* **1991**, *251* (4996), 905−914.

(23) Milner, T.; Witten, T. A.; Cates, M. E. Theory of the grafted polymer brush. *Macromolecules* **1988**, *21* (8), 2610−2619.

(24) Eichmann, S. L.; Meric, G.; Swavola, J. C.; Bevan, M. A. Diffusing Colloidal Probes of Protein-Carbohydrate Interactions. *Langmuir* **2013**, *29* (7), 2299−2310.

(25) Murphy, T. J.; Aguirre, J. L. Brownian Motion of N Interacting Particles.1. Extension of Einstein Diffusion Relation to N-Particle Case. *J. Chem. Phys.* **1972**, *57* (5), 2098.

(26) Brenner, H. The Slow Motion of a Sphere Through a Viscous Fluid Towards a Plane Surface. *Chem. Eng. Sci.* **1961**, *16* (3−4), 242−251.

(27) Bevan, M. A.; Prieve, D. C. Hindered Diffusion of Colloidal Particles Very Near to A Wall: Revisited. *J. Chem. Phys.* **2000**, *113* (3), 1228−1236.

(28) Crocker, J. C.; Grier, D. G. Methods of Digital Video Microscopy for Colloidal Studies. *J. Colloid Interface Sci.* **1996**, *179*, 298−310.

(29) Beltran-Villegas, D. J.; Sehgal, R. M.; Maroudas, D.; Ford, D. M.; Bevan, M. A. Fokker−Planck Analysis of Separation Dependent Potentials and Diffusion Coefficients in Simulated Microscopy Experiments. *J. Chem. Phys.* **2010**, *132*, 044707.

(30) Beltran-Villegas, D. J.; Edwards, T. D.; Bevan, M. A. Self-Consistent Colloidal Energy and Diffusivity Landscapes in Macromolecular Solutions. *submitted* **2013**.

(31) Kopelevich, D. I.; Panagiotopoulos, A. Z.; Kevrekidis, I. G. Coarse-grained kinetic computations for rare events: Application to micelle formation. *J. Chem. Phys.* **2005**, *122*, 044908.

(32) Hummer, G. Position-dependent diffusion coefficients and free energies from Bayesian analysis of equilibrium and replica molecular dynamics simulations. *New J. Phys.* **2005**, *7*, 34.

(33) Li, H. C.; De Bruyn, P. L. Electrokinetic and adsorption studies on quartz. *Surf. Sci.* **1966**, *5* (2), 203−220.

(34) James, R. O. Characterization of Colloids in Aqueous Systems. *Adv. Ceram.* **1987**, *21*, 349−410.

(35) Parsegian, V. A.; Weiss, G. H. Spectroscopic Parameters for Computation of van der Waals Forces. *J. Colloid Interface Sci.* **1981**, *81*, 285−289.
(36) Wu, H.-J.; Pangburn, T. O.; Beckham, R. E.; Bevan, M. A. Measurement and Interpretation of Particle−Particle and Particle−Wall Interactions in Levitated Colloidal Ensembles. *Langmuir* **2005**, *21* (22), 9879−9888.
(37) Prieve, D. C. Measurement of Colloidal Forces with TIRM. *Adv. Colloid Interface Sci.* **1999**, *82* (1−3), 93−125.
(38) Oetama, R. J.; Walz, J. Y. Simultaneous investigation of sedimentation and diffusion of a single colloidal particle near an interface. *J. Chem. Phys.* **2006**, *124* (16), 164713.
(39) Pagac, E. S.; Tilton, R. D.; Prieve, D. C. Hindered Mobility Of A Rigid Sphere Near A Wall. *Chem. Eng. Commun.* **1996**, *148*, 105.
(40) Vold, M. J. The Effect of Adsoprtion on the van der Waals Interaction of Spherical Colloidal Particles. *J. Colloid Sci.* **1961**, *16*, 1−12.
(41) Parsegian, V. A. Model for van der Waals Attraction between Sphereical Particles with Nonuniform Adsorbed Polymer. *J. Colloid Interface Sci.* **1975**, *51* (3), 543−546.
(42) Bevan, M. A.; Petris, S. N.; Chan, D. Y. C. Solvent quality dependent continuum van der Waals attraction and phase behavior for colloids bearing nonuniform adsorbed polymer layers. *Langmuir* **2002**, *18* (21), 7845−7852.
(43) Napper, D. H. *Polymeric Stabilization of Colloidal Dispersions*; Academic Press: New York, 1983.
(44) Odiachi, P. C.; Prieve, D. C. Total internal reflection microscopy: Distortion caused by additive noise. *Ind. Eng. Chem. Res.* **2002**, *41* (3), 478−485.
(45) Odiachi, P. C.; Prieve, D. C. Removing the effects of additive noise from TIRM measurements. *J. Colloid Interface Sci.* **2004**, *270* (1), 113−122.
(46) Bevan, M. A.; Prieve, D. C. Forces and hydrodynamic interactions between polystyrene surfaces with adsorbed PEO-PPO-PEO. *Langmuir* **2000**, *16* (24), 9274−9281.
(47) Dagastine, R. R.; Bevan, M. A.; White, L. R.; Prieve, D. C. Calculation of van der Waals forces with diffuse coatings: Applications to roughness and adsorbed polymers. *J. Adhes.* **2004**, *80* (5), 365−394.
(48) Zhulina, E. B.; Klein Wolterink, J.; Borisov, O. V. Screening Effects in a Polyelectrolyte Brush: Self-Consistent-Field Theory. *Macromolecules* **2000**, *33* (13), 4945−4953.
(49) Fleer, G. J.; Stuart, M. A. C.; Scheutjens, J. M. H. M.; Cosgrove, T.; Vincent, B. *Polymers at Interfaces*; Chapman & Hall: New York, 1993.
(50) Israelachvili, J. N., *Intermolecular and Surface Forces*, 2nd ed.; Academic Press: New York, 1992; p 450.
(51) Zhulina, E. B.; Borisov, O. V.; Pryamitsyn, V. A.; Birshtein, T. M. Coil-Globule Type Transitions in Polymers. 1. Collapse of Layers of Grafted Polymer Chains. *Macromolecules* **1991**, *24*, 140.